Polymer:Fullerene Bimolecular Crystals for Near-Infrared Spectroscopic Photodetectors

Zheng Tang,* Zaifei Ma, Antonio Sánchez-Díaz, Sascha Ullbrich, Yuan Liu, Bernhard Siegmund, Andreas Mischok, Karl Leo, Mariano Campoy-Quiles, Weiwei Li,* and Koen Vandewal*

Spectroscopic photodetection is a powerful tool in disciplines such as medical diagnosis, industrial process monitoring, or agriculture. However, its application in novel fields, including wearable and biointegrated electronics, is hampered by the use of bulky dispersive optics. Here, solution-processed organic donor–acceptor blends are employed in a resonant optical cavity device architecture for wavelength-tunable photodetection. While conventional photodetectors respond to above-gap excitation, the cavity device exploits weak subgap absorption of intermolecular charge-transfer states of the intercalating poly[2,5-bis(3-tetradecylthiophen-2-yl)thieno[3,2-b]thiophene] (PBTTT):[6,6]-phenyl-C61-butyric acid methyl ester (PCBM) bimolecular crystal. This enables a highly wavelength selective, near-infrared photoresponse with a spectral resolution down to 14 nm, as well as dark currents and detectivities comparable with commercial inorganic photodetectors. Based on this concept, a miniaturized spectrophotometer, comprising an array of narrowband cavity photodetectors, is fabricated by using a blade-coated PBTTT:PCBM thin film with a thickness gradient. As an application example, a measurement of the transmittance spectrum of water by this device is demonstrated.

Spectrophotometric methodologies are widely employed for resolving chemical compositions in medical diagnosis, environmental monitoring, agricultural production, astronomical investigation, imaging, and surveillance.[1,2] Traditional

Dr. Z. Tang, Dr. Z Ma, S. Ullbrich, Y. Liu, B. Siegmund, Dr. A. Mischok,
Prof. K. Leo, Prof. K. Vandewal
Dresden Integrated Center for Applied Physics and Photonic
Materials (IAPP) and Institute for Applied Physics
Technische Universität Dresden
Dresden 01187, Germany
E-mail: zheng.tang@iapp.de; koen.vandewal@iapp.de
Dr. A. Sánchez-Díaz, Dr. M. Campoy-Quiles
Institut de Ciència de Materials de Barcelona (ICMAB-CSIC)
Campus de la UAB, Bellaterra 08193, Spain
Prof. W. Li
Beijing National Laboratory for Molecular Sciences
CAS Key Laboratory of Organic Solids
Institute of Chemistry
Chinese Academy of Sciences
Beijing 10090, P. R. China
E-mail: liweiwei@iccas.ac.cn

spectrometers are based on broadband photodetectors combined with diffraction gratings or dichroic prisms,[1] characterized by a rather high structural complexity and cost. This can be circumvented using an array of photodetectors, sensitive at specific wavelengths, allowing for a miniaturization and new applications, such as wearable electronics and biomedical implementation. However, such arrays demand a significant advance in the development of photodetectors, with key requirements including a narrow spectral response, continuously tunable detection wavelengths, and ease of integration. Furthermore, the device architecture should be simple and achievable with a low-cost deposition technique using abundant, nontoxic materials.

Solution processable organic bulk-heterojunctions (BHJs)[3] or metal-halide perovskites[4] are in this respect interesting candidates, and several approaches to achieve wavelength-selective photodetection using these materials have been recently proposed.[5,6] For photoactive materials with tailored absorption spectra, high responsivities were achieved in the short-wavelength regime (<700 nm), with a spectral full-width at half-maximum (FWHM) of the order of 100 nm.[7–11] Narrower spectral responses were recently demonstrated through the use of thick active layers, resulting in carrier collection only for weakly absorbed wavelengths at the optical gap.[12–14]

Despite these recent developments, the reported narrowband detectors operate mostly in the visible range, with limited external quantum efficiencies (EQEs) (<10%). More importantly, the previously proposed device concepts are fundamentally limited on the wide-range spectral tunability, which hinders their capability for spectroscopic applications.

An elegant alternative approach makes use of optical cavity effects.[15] By sandwiching a weakly absorbing photoactive layer in-between two (partially) reflecting electrodes, narrow spectral resonances at specific wavelengths can be achieved.[16–18] In this case, detection wavelengths are determined by the cavity thickness. However, typical organic semiconductors are too strongly absorbing to provide high-quality, narrow cavity resonances for above-gap wavelengths. In a donor–acceptor blend,

the intermolecular charge-transfer (CT) states, on the other hand, provide weak absorption in the subgap region. This has led to FWHM values down to 40 nm with EQE over 10% in the 850–950 nm range, which is in the CT absorption region of the used Zn-phthalocyanine:C_{60} blends.[19] An additional advantage of exploiting the intermolecular CT absorption band is that the detection wavelengths can extend far beyond those of the neat absorber materials. This allows for near-infrared (NIR) detection without the synthesis of new organic absorbers.

In this work, solution-processed polymer cavity photodetectors that exploit the CT absorption, with low dark currents and specific detectivities (D^*) approaching commercial Si photodetectors, are realized. By evaluating the cavity optics, we propose material selection rules allowing for a simple device architecture in which a single absorber layer is sandwiched between mirroring electrodes. Using a poly[2,5-bis(3-tetradecylthiophen-2-yl)thieno[3,2-b]thiophene] (PBTTT):[6,6]-phenyl-C61-butyric acid methyl ester (PCBM) blend, we achieve an FWHM of 14 nm. Due to its intercalating nature, PBTTT:PCBM has an appropriate CT absorption strength, which enables us to realize EQEs higher than 20% for wavelengths up to 960 nm, which is more than

300 nm below the optical gap of PBTTT. Furthermore, prototype miniaturized spectrometers for the wavelength range 700–1100 nm are successfully constructed using a blade-coated PBTTT:PCBM layer with a thickness wedge (i.e., a gradient). The simplicity in device construction and excellent performance along with the advantages of organic materials, such as low toxicity, flexibility, and scalability, make this class of photodetectors highly interesting for innovative areas of spectroscopic applications, not compatible with present photodetecting technologies.

Organic donor–acceptor BHJ blends are easily integrated into a resonant optical cavity device architecture. A schematic picture of the device architecture is shown in **Figure 1**a. The mirrors on both sides of the BHJ active layer simultaneously act as electrodes, modified by ultrathin interlayers to achieve the desired work function. In this work, polyethylenimine (PEIE)[20] (<1 nm) is used to lower the work function of the electron-collecting bottom Au or Ag electrode. A 10-nm MoO_3 layer is used to provide hole selectivity to the top Ag electrode.

For such cavity devices, maximum field enhancement is reached at a resonance wavelength λ_m that depends to a good approximation on the thickness L and the refractive index n of the organic layer sandwiched between the metals[17]
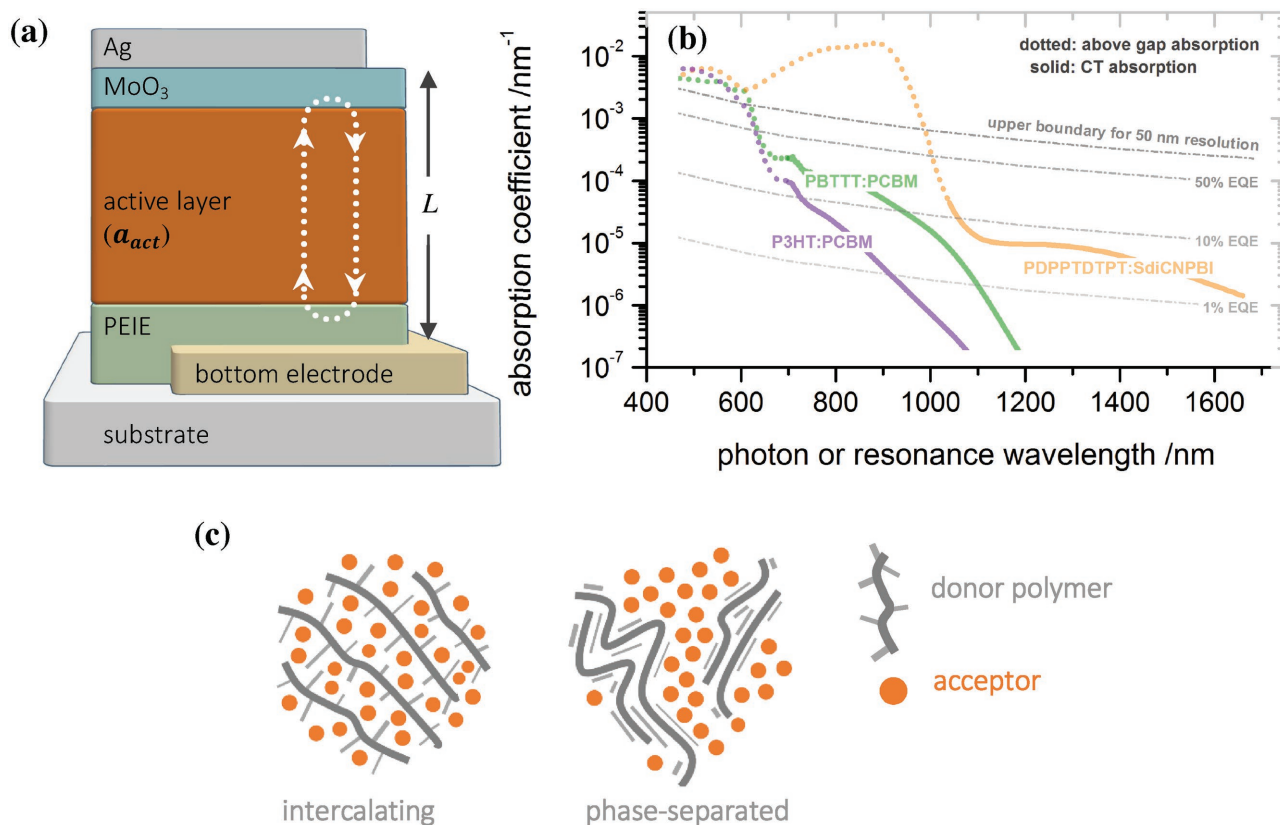

Figure 1. a) Schematic device architecture of a resonant-cavity-enhanced organic BHJ photodetector. The resonance wavelength is tuned by varying the thickness of the active layer. The metal–metal cavity detectors studied in this work have a semitransparent Au bottom electrode and a nontransparent Ag top electrode. The devices based on DBRs have a semitransparent top Ag electrode, and a bottom DBR mirror modified by conductive PEDOT:PSS PH1000. b) Absorption coefficients of P3HT:PCBM 1:1 (weight ratio), PBTTT:PCBM 1:4, and PDPPTDTPT:SdiCNPBI 1:1. The upper and lower boundaries for the active layer absorption coefficient enabling a spectral FWHM <50 nm and a maximum EQE above 1%, 10%, and 50% are indicated by gray dash-dotted lines. c) A schematic representation of an intercalated and nonintercalated BHJ polymer/fullerene (donor/acceptor) system. The degree of intermixing between the donor and acceptor materials determines the CT absorption strength.

**ADVANCED
SCIENCE NEWS**

www.advancedsciencenews.com

**ADVANCED
MATERIALS**

www.advmat.de

$$\lambda_{\mathrm{m}} = \frac{2Ln}{m} \qquad (1)$$

Here, the order of the resonance, m, is a natural number (>0). Simply adjusting the cavity thickness L allows a continuous tuning of the resonant wavelength for photodetection.

The FWHM of the photoresponse of such a cavity device is strongly related to the absorption strength of the active layer as well as parasitic absorption losses in the interlayers and mirrors. In an ideal cavity, the FWHM is proportional to the effective absorption coefficient α of the cavity system, which includes the absorption coefficient of the active layer a_{act}, and parasitic absorption (Section SI-2, Supporting Information)

$$\mathrm{FWHM} \approx \frac{\alpha \lambda_{\mathrm{m}}^2}{n\pi} \qquad (2)$$

Using Equation (2), we can derive an upper limit for the absorption coefficient of the active layer a_{act}, ensuring narrowband absorption with an FWHM of the EQE no larger than 50 nm (Figure 1b).

Using optical cavities, the EQE values at the resonance peaks can, in principle, be unity, but are practically reduced by parasitic absorption in the reflecting electrodes and a nonunity internal quantum efficiency (IQE). The maximum achievable EQE (EQE$_{\mathrm{max}}$) is given by

$$\mathrm{EQE_{max}} = \frac{a_{\mathrm{act}}}{a_{\mathrm{act}} + \dfrac{2\tau}{L}} \qquad (3)$$

where τ is the effective optical depth (unitless) responsible for absorption losses in the mirrors (derived in Section SI-2 in the Supporting Information). For noble metal mirrors, such as Ag and Au, $2\tau \approx 0.05$. Equation (3) allows us to determine lower boundaries for a_{act}. In Figure 1b, these are shown for target EQE$_{\mathrm{max}}$ values of 1%, 10%, and 50%, respectively.

A close look at Figure 1b shows that the absorption coefficient of a typical neat organic absorber ($\alpha > 10^{-3}$ nm^{-1}) is too high to achieve narrowband ($<$50 nm) cavity enhancement. The subgap interfacial CT states formed at the interface between the donor and the acceptor have intrinsically lower absorption coefficients,[21–23] allowing, in principle, very narrow peaks. However, using noble metal electrodes, of which the parasitic absorption is much higher than the typical CT absorption, considerably limits the peak EQE, especially for longer wavelengths. For instance, as shown in Figure 1b, the absorption coefficient of a standard BHJ blend based on poly(3-hexylthiophene-2,5-diyl) (P3HT)[24] and PCBM falls in between the upper boundary for 50 nm FWHM and the lower one for 10% EQE, but only in a narrow wavelength range between 650 and 750 nm.

To exploit the full potential of the device architecture shown in Figure 1a, the absorption strength of the CT state, therefore, needs to be increased. Since it is proportional to the density of CT complexes or the density of donor–acceptor contacts,[25] blends with a high degree of intermixing between donor and acceptor materials are desired. In this respect, the semicrystalline polymer, PBTTT,[26–28] has a structural advantage over P3HT, since it favors the intercalation of fullerene molecules between its side chains and the formation of bimolecular crystals.[29,30] While for P3HT:PCBM the lowest energy CT state is formed at the interface between aggregates of P3HT and PCBM,[31] the highly intermixed PBTTT:PCBM blend has its lowest energy CT state within the co-crystal (Figure 1c). As compared to P3HT, PBTTT has a similar optical gap (absorption onset at 650 nm) and a similar CT state energy ($E_{\mathrm{CT}} \approx 1.15$ eV; Figure S5, Supporting Information). However, PBTTT:PCBM shows significantly stronger CT absorption than P3HT:PCBM (Figure 1b), allowing for a wider spectral window (650–950 nm) for resonant cavity effects, with expected EQEs over 10%.

We now demonstrate organic photodetectors based on BHJ systems with CT absorption enhanced by the simple metal–metal cavity (glass/Au 30 nm/PEIE 1 nm/PBTTT:PCBM/MoO$_3$ 10 nm/Ag 100 nm) of Figure 1a. The thickness of the semitransparent Au mirror is optimized using a transfer matrix (TM) simulation,[32] taking into account the effect of standing waves between the reflecting electrodes and their parasitic absorption losses. As shown in **Figure 2**a, the measured EQE spectra of the PBTTT:PCBM detectors are in good agreement with the simulated results. The slightly lower experimental EQE peak values can be ascribed to nonunity IQE or thin-film roughness, diminishing the cavity effect (Figure S6, Supporting Information). The continuous first-order resonance wavelength tuning in the range between 700 and 1000 nm is realized by varying the thickness of the active layer from 115 to 190 nm. In this range, the EQE values are indeed over 10%, with FWHM $<$ 50 nm. Note that the above-gap absorption of PBTTT contributes to the response at wavelengths shorter than 700 nm. To realize truly narrowband detection, this above-gap absorption is easily suppressed by an additional PBTTT layer above the Au mirror, as shown in Figure S7 (Supporting Information).

Furthermore, metal–metal cavity photodetectors based on the P3HT:PCBM system as well as on the poly[3-(5-(4-(2-ethylhexyl)-4H-dithieno[3,2-b:2′,3′-d]pyrrol-2-yl)thiophen-2-yl)-2,5-bis(2-hexyldecyl)-6-(thiophen-2-yl)-2,5-dihydropyrrolo[3,4-c]pyrrole-1,4-dione]:1,1′,3,3′,8,8′,10,10′-octaoxo-2,2′,9,9′-tetra(undecan-6-yl)-1,1′,2,2′,3,3′,8,8′,9,9′,10,10′-dodecahydro-[5,5′-bianthra[2,1,9-def:6,5,10-d′e′f′]diisoquinoline]-13,13′-dicarbonitrile (PDPPTDTPT:SdiCNPBI)[33,34] blend are fabricated. For the latter, with a low E_{CT} ($\approx$ 0.7 eV), detection wavelengths are easily extended to a remarkable range of 1000–1700 nm (details in Sections SI-3 and SI-4, Supporting Information), which is among the longest detection wavelengths reported for organic photodetectors.[42–46] However, due to the absence of intercalation,[30] both blend systems result in photodetectors with low EQE ($<$10%), agreeing well with the results shown in Figure 1b.

The TM simulations for the PBTTT:PCBM devices reveal that, at the first-order resonance, the EQE and spectral selectivity are still strongly limited by parasitic absorption in the electrodes (Figure S8, Supporting Information). According to Equation (3), the effect of these parasitic absorption losses can be reduced by increasing the order of resonance ($m > 1$), using thicker active layers. This is indeed the case—Figure 2 shows the remarkable benefit of using second-order resonances: we obtain much higher EQE values (20–40%, Figure 2b) with FWHM values as small as 20 nm (Figure 2c). An added
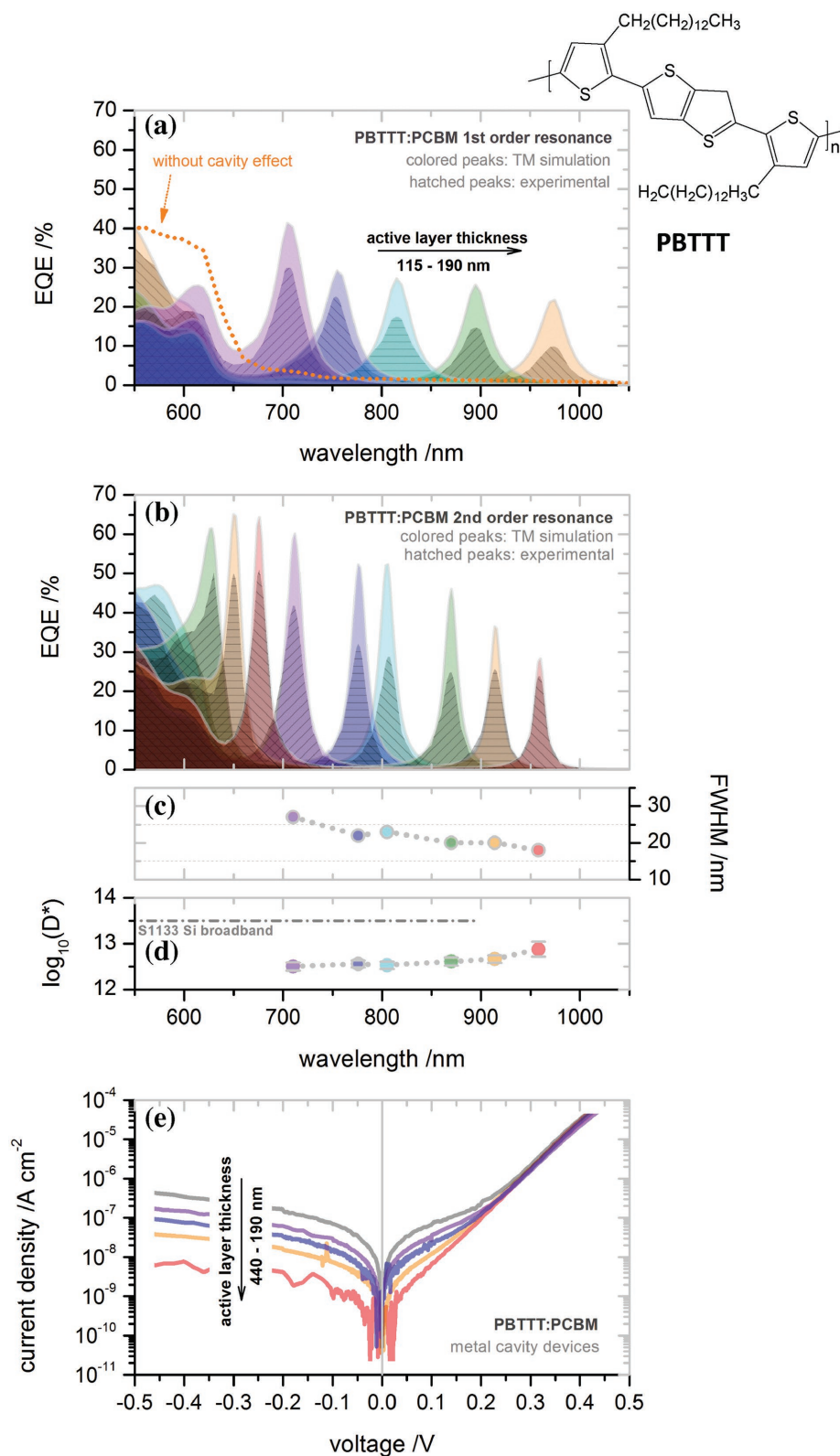
ADVANCED
SCIENCE NEWS

www.advancedsciencenews.com

ADVANCED
MATERIALS

www.advmat.de

Figure 2. Performance of photodetectors based on PBTTT:PCBM (1:4) in a metal–metal cavity structure. Measured EQE and TM simulation predicted EQE (assuming an IQE of 100%) for devices with an active layer thicknesses varied between a) 115 and 190 nm for first-order resonances, and b) 290 and 440 nm for second-order resonances. c) FWHM and d) calculated specific detectivity D* (Jones) of the devices at second-order resonances. The detectivity of a commercial Si-based broadband photodetector (S1133, Hamamatsu) is also given for comparison. e) Dark JV characteristic curves of the devices with different active layer thicknesses.

important advantage is the significant suppression of parasitic shunt currents.[35] As shown in Figure 2e, there is a clear dependence of the shunt resistance on the active layer thickness. From the current density–voltage (JV) characteristics of the device with a 400-nm active layer thickness, we derive a shunt resistance as high as 50 MΩ cm^2. In fact, shunt losses can barely be measured in the JV curve of the thickest device, and the dark current under a small voltage bias is dominated by the dark saturation current related to the intrinsic diode properties of the device. This leads to very low Johnson and shot noise currents (Table S1, Supporting Information).

The specific detectivity $D*$ of a photodetector depends on the geometry of the electrodes, the shape of the active area, as well as the measurement circuit and shielding from environmental noise. Focusing in this work on the device concept, we calculate the maximum achievable $D*$ at zero voltage bias (details in Section SI-1, Supporting Information), assuming only the presence of Johnson noise. At the second-order resonance wavelength close to 1000 nm, $D*$ is over 10^{13} Jones (Figure 2d). This suggests that the performance of the cavity photodetectors based on PBTTT:PCBM approaches that of commercial broadband silicon detectors.[35]

Figure 3a shows the photocurrent of the PBTTT:PCBM device with its second-order resonance of 1000 nm, as a function of irradiance. When exciting at the resonance wavelength, the photoresponse is found to be strictly linear over 6.5 orders of magnitude, corresponding to a linear dynamic range of at least 130 dB, comparable to that of inorganic photodetectors.[35,36] At very low light intensities, the photoresponse is limited by the sensitivity of our measurement setup. For irradiances above 10 mW cm^{-2}, a slightly sublinear response is observed due to bimolecular recombination.[37]

The response time of the cavity device, with a second-order resonance at 1000 nm (active layer thickness = 440 nm, active area = 0.5 mm^2), is measured under 25 ps pulsed laser excitation. As shown in Figure 3b, the device has a fall time (from 90% to 10%) of $\approx$ 230 ns and a 3 dB bandwidth of over 1 MHz at short-circuit conditions, which are certainly sufficiently fast for a detector array readout.

The use of noble metal thin films acting simultaneously as a (semitransparent) mirror and electrode introduces a considerable amount of parasitic absorption, limiting device performance, even for the second-order resonance devices. Further improvement thus requires alternative (nonmetal) reflecting electrodes with higher reflectivity and lower parasitic absorption losses. Below, we demonstrate devices in which high-conductivity poly(3,4-ethylenedioxythiophene):polystyrene sulfonate (PEDOT:PSS PH1000) coated distributed Bragg reflectors (DBRs) are used as the back reflecting electrode. The DBRs are based on 21 alternating TiO$_2$ and SiO$_2$ layers (TiO$_2$ being the top layer),[38] with a reflectance over 99.9% within the stopbands. The stopbands are in the range of 650–800 and 750–900 nm (Figure S9, Supporting Information), well suited for the CT state absorption of PBTTT:PCBM.

The DBR cavity devices have an architecture of glass/DBR/PEDOT:PSS PH1000 (20 nm)/PEIE (1 nm)/PBTTT:PCBM/MoO$_3$ (10 nm)/Ag (30 nm). The PEIE-modified, electron collecting PEDOT electrode[39] is thin enough to avoid significant parasitic absorption losses, while still sufficiently conductive in
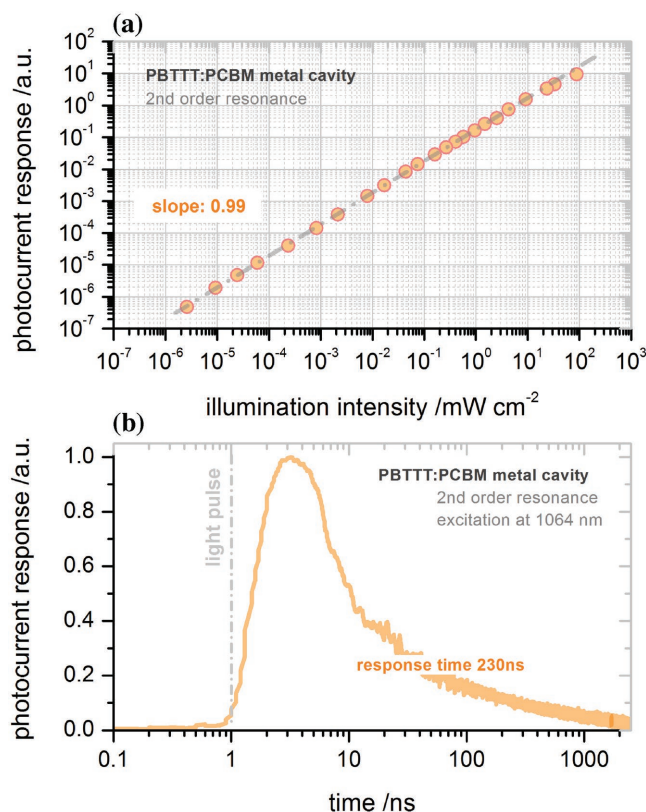

Figure 3. Photocurrent response of a photodetector based on PBTTT:PCBM (1:4) in a metal–metal cavity. The current response of a device with a resonance wavelength of 1000 nm (second order) is measured as a function of a) illumination intensity and b) time. The transient signal is recorded upon an NIR laser excitation starting at 1 ns, with an excitation pulse length of 25 ps. The response time is derived from the 90–10% signal fall time. The device, with an active area of 0.5 mm^2 and an active layer thickness of 440 nm, was measured at short-circuit conditions.

the lateral direction. EQEs of second-order resonance devices on DBRs are shown in **Figure 4**a. Compared to photodetectors based on a metal–metal cavity, the spectral selectivity of the DBR devices is further improved. The spectral line FWHM value is further reduced to 14 nm (Figure 4b), which is the lowest value for organic narrowband photodetectors to date.

It should be further stressed that the high spectral selectivity is achieved without compromising on specific detectivity. In fact, we find that the JV curves of the detectors based on DBRs are similar to those based on metal mirrors with the same active materials system (Figure S10, Supporting Information). This leads, also for the DBR-based detectors, to a calculated specific detectivity close to 10^{13} Jones (Figure 4c).

Figure 5a displays a schematic picture and a photograph of a proof-of-concept miniature spectrometer consisting of an array of metal–metal cavity photodetectors based on PBTTT:PCBM. Due to the thickness gradient in the active layer, each pixel has a different resonance wavelength, enabling spectroscopic photodetection with a resolution related to the FWHM of the individual photodetectors. The thickness gradient of the PBTTT:PCBM active layer is achieved by blade coating with a linearly decreasing coating speed. Coating conditions (details
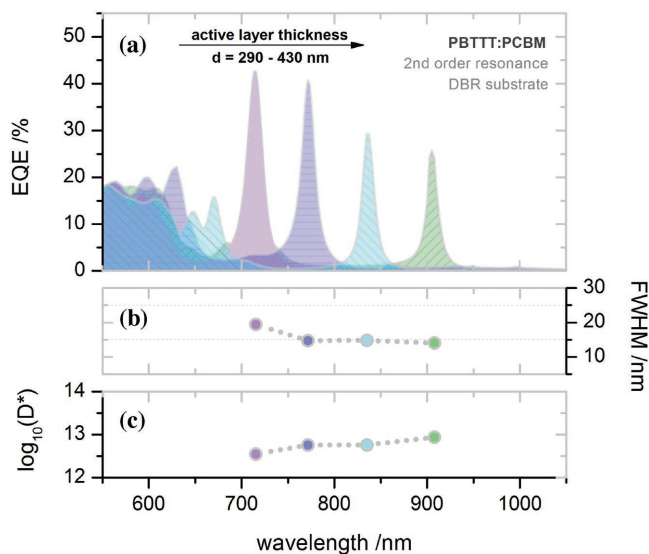
**ADVANCED
SCIENCE NEWS**
www.advancedsciencenews.com

**ADVANCED
MATERIALS**
www.advmat.de

Figure 4. Performance of cavity-enhanced photodetectors based on DBRs and PBTTT:PCBM (1:4). a) EQE, b) FWHM, and c) specific detectivity $D*$ (Jones) for devices with a second-order resonance. Device architecture: glass/DBR/PEDOT:PSS PH1000 (20 nm)/PEIE (1 nm)/PBTTT:PCBM/MoO$_3$ (10 nm)/Ag (30 nm).

in Section SI-1 in the Supporting Information) are optimized to achieve a thickness variation from 100 to 200 nm over a distance of 6 cm, resulting in first-order resonance wavelengths in the range of 700–1100 nm. The spectral responses of the photodetectors are given in Figure S11 (Supporting Information).

In order to demonstrate that this device has a sufficient spectral resolution for a potential application in moisture detection, the transmittance spectrum of water was measured using a miniature spectrometer and a xenon lamp as the light source (Figure 5b). The transmission feature at 970 nm, corresponding to the first vibrational overtone of the O−H bond absorption, can be clearly identified. Compared to the spectrum measured by a commercial spectrometer, only small differences are observed. Such organic cavity spectrometers can thus provide a simple and cheap alternative for inline moisture monitoring, a key component in wood, paper, concrete, and pharmaceutical industries.

The presented proof-of-concept device demonstrates a combination of wide spectroscopic photodetection and compactness with potential for a fast readout, as well as a simple and cheap fabrication method, which cannot be easily achieved with other technologies. A further miniaturization of the spectrometer will require reducing the photodetecting pixel size and spacing, and
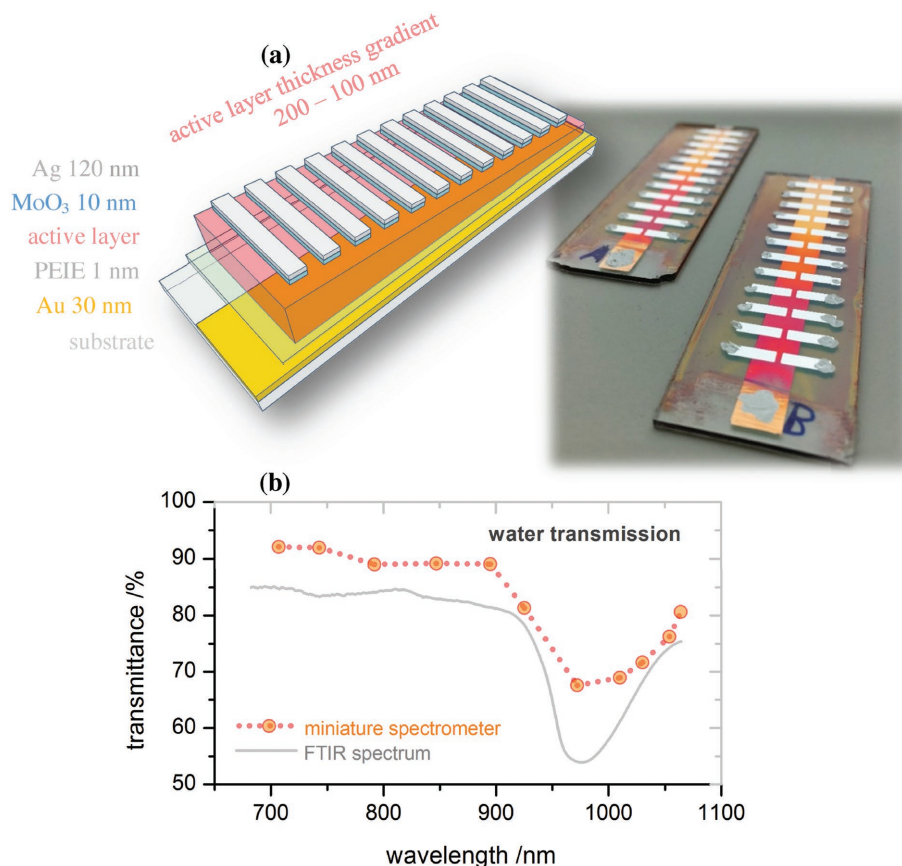

Figure 5. Miniature NIR spectrometer with a thickness-wedged PBTTT:PCBM layer in a metal–metal cavity. a) A photograph of the spectrometers fabricated in this work and a schematic picture of the device architecture. The spectrometer is based on a single-wedged active layer, resulting in different resonance wavelengths for each individual detecting pixel. The change in active layer color is the result of the gradually changing interference conditions. b) Water transmittance spectrum measured by the spectrometer constructed in this work in comparison to a spectrum measured by a commercial Fourier transform infrared spectrometer.

alternative deposition techniques to achieve thickness-wedged layers over smaller distances. In this respect, slot-die or inkjet coating seems useful,[40] allowing us to control the active layer thickness by ink injection speed.

In summary, although the performance of the miniature spectrometer is limited by parasitic absorption losses in the metal electrodes, these losses can be reduced by using less absorbing mirrors and moving to higher order resonances. As we demonstrated, with second-order resonances (Figure 2) or DBRs (Figure 4), the performance of organic cavity detectors based on PBTTT:PCBM CT absorption is superior, as compared to previously reported narrowband photodetectors based on organic or perovskite materials.[13,14] Furthermore, as compared to evaporated small molecule cavity detectors,[18,19] requiring thin active layers for charge transport, we achieve lower parasitic absorption losses and lower dark currents using thick polymer–fullerene blends. This leads to a significantly higher specific detectivity, enhanced spectral selectivity, easier spectral tenability, and a simpler device architecture. In fact, these solution-processed BHJ cavity detectors have in many aspects comparable performance to commercial silicon-based detectors,[35] with the latter lacking in spectral tunability and selectivity.

The presented approach is particularly interesting in the NIR region of the electromagnetic spectrum, where the CT bands of most donor–acceptor combinations, developed for organic solar cells, are found.[21,41] By varying the combination of donor and acceptor materials, the CT absorption can be easily tuned up to 1700 nm, as we demonstrated with the PDPPTDTPT:SdiCNPBI system (details in Section SI-4, Supporting Information). Tunability over a range of 700 nm demonstrates the potential of organic materials for wavelength-selective photodetection far in the NIR.[42–46] More importantly, our novel approach for extending the photodetection range is considerably simpler than other conventional methods that require the development of new absorbers with very low optical gaps, for which then a suitable acceptor is to be found.

We expect future research to focus on performance improvements for wavelengths beyond 1100 nm. New, promising BHJ candidates being used as the active material system for cavity-enhanced detectors should not only have proper energy levels, but should also intercalate significantly on the molecular level to facilitate a large number of photoactive interfacial CT states. While the PBTTT:PCBM co-crystal has been successfully used as a model system for fundamental studies on organic photovoltaics,[29] we anticipate future applications of such intercalating crystals in cavity detectors and spectrometers, spanning the entire visible to the NIR region.

Experimental Section

Details of "Experimental Section" are provided in the Supporting information.

Supporting Information

Supporting Information is available from the Wiley Online Library or from the author.

Conflict of Interest

The authors declare no conflict of interest.

[1] C. P. Bacon, Y. Mattley, R. D. Frece, *Rev. Sci. Instrum.* **2003**, *75*, 1.

[2] F. P. G. de Arquer, A. Armin, P. Meredith, E. H. Sargent, *Nat. Rev. Mater.* **2017**, *2*, 16100.

[3] G. Yu, J. Gao, J. C. Hummelen, F. Wudl, A. J. Heeger, *Science* **1995**, *270*, 1789.

[4] A. Kojima, K. Teshima, Y. Shirai, T. Miyasaka, *J. Am. Chem. Soc.* **2009**, *131*, 6050.

[5] K. J. Baeg, M. Binda, D. Natali, M. Caironi, Y. Y. Noh, *Adv. Mater.* **2013**, *25*, 4267.

[6] R. D. Jansen-van Vuuren, A. Armin, A. K. Pandey, P. L. Burn, P. Meredith, *Adv. Mater.* **2016**, *28*, 4766.

[7] T. Rauch, M. Böberl, S. F. Tedde, J. Fürst, M. V. Kovalenko, G. Hesser, U. Lemmer, W. Heiss, O. Hayden, *Nat. Photonics* **2009**, *3*, 332.

[8] R. Jansen van Vuuren, K. D. Johnstone, S. Ratnasingam, H. Barcena, P. C. Deakin, A. K. Pandey, P. L. Burn, S. Collins, I. D. W. Samuel, *Appl. Phys. Lett.* **2010**, *96*, 253303.

[9] Y. Higashi, K. S. Kim, H.-G. Jeon, M. Ichikawa, *J. Appl. Phys.* **2010**, *108*, 034502.

[10] K. H. Lee, G. H. Lee, D.-S. Leem, J. Lee, J. W. Chung, X. Bulliard, H. Choi, K. B. Park, K. S. Kim, Y. W. Jin, S. Lee, S. Y. Park, *J. Phys. Chem. C* **2014**, *118*, 13424.

[11] M. G. Han, K. B. Park, X. Bulliard, G. H. Lee, S. Yun, D. S. Leem, C. J. Heo, T. Yagi, R. Sakurai, T. Ro, S. J. Lim, S. Sul, K. Na, J. Ahn, Y. W. Jin, S. Lee, *ACS Appl. Mater. Interfaces* **2016**, *8*, 26143.

[12] A. Armin, R. D. J. Vuuren, N. Kopidakis, P. L. Burn, P. Meredith, *Nat. Commun.* **2015**, *6*, 6343.

[13] Q. Lin, A. Armin, P. L. Burn, P. Meredith, *Nat. Photonics* **2015**, *9*, 687.

[14] Y. Fang, Q. Dong, Y. Shao, Y. Yuan, J. Huang, *Nat. Photonics* **2015**, *9*, 679.

**ADVANCED
SCIENCE NEWS**

www.advancedsciencenews.com

**ADVANCED
MATERIALS**

www.advmat.de

[15] K. J. Vahala, *Nature* **2003**, *424*, 839.

[16] K. Kishino, M. S. Unlu, J. I. Chyi, J. Reed, L. Arsenault, H. Morkoc, *IEEE J. Quantum Electron.* **1991**, *27*, 2025.

[17] M. S. Ünlü, S. Strite, *J. Appl. Phys.* **1995**, *78*, 607.

[18] K. H. An, B. O'Connor, K. P. Pipe, M. Shtein, *Org. Electron.* **2009**, *10*, 1152.

[19] B. Siegmund, A. Mischok, J. Benduhn, Z. Olaf, N. Frederik, S. Donato, F. Hartmut, K. Christian, *Nat. Commun.* **2017**, DOI: 10.1038/ncomms15421.

[20] Y. Zhou, C. Fuentes-Hernandez, J. Shim, J. Meyer, A. J. Giordano, H. Li, P. Winget, T. Papadopoulos, H. Cheun, J. Kim, M. Fenoll, A. Dindar, W. Haske, E. Najafabadi, T. M. Khan, H. Sojoudi, S. Barlow, S. Graham, J.-L. Brédas, S. R. Marder, A. Kahn, B. Kippelen, *Science* **2012**, *336*, 327.

[21] K. Vandewal, K. Tvingstedt, A. Gadisa, O. Inganäs, J. V. Manca, *Nat. Mater.* **2009**, *8*, 904.

[22] K. Vandewal, *Annu. Rev. Phys. Chem.* **2016**, *67*, 113.

[23] K. Vandewal, S. Albrecht, E. T. Hoke, K. R. Graham, J. Widmer, J. D. Douglas, M. Schubert, W. R. Mateker, J. T. Bloking, G. F. Burkhard, A. Sellinger, J. M. J. Fréchet, A. Amassian, M. K. Riede, M. D. McGehee, D. Neher, A. Salleo, *Nat. Mater.* **2014**, *13*, 63.

[24] F. Padinger, R. S. Rittberger, N. S. Sariciftci, *Adv. Funct. Mater.* **2003**, *13*, 85.

[25] K. Vandewal, K. Tvingstedt, A. Gadisa, O. Inganäs, J. V. Manca, *Phys. Rev. B* **2010**, *81*, 125204.

[26] I. McCulloch, M. Heeney, C. Bailey, K. Genevicius, I. MacDonald, M. Shkunov, D. Sparrowe, S. Tierney, R. Wagner, W. Zhang, M. L. Chabinyc, R. J. Kline, M. D. McGehee, M. F. Toney, *Nat. Mater.* **2006**, *5*, 328.

[27] E. Buchaca-Domingo, K. Vandewal, Z. Fei, S. E. Watkins, F. H. Scholes, J. H. Bannock, J. C. de Mello, L. J. Richter, D. M. DeLongchamp, A. Amassian, M. Heeney, A. Salleo, N. Stingelin, *J. Am. Chem. Soc.* **2015**, *137*, 5256.

[28] J. E. Parmer, A. C. Mayer, B. E. Hardin, S. R. Scully, M. D. McGehee, M. Heeney, I. McCulloch, *Appl. Phys. Lett.* **2008**, *92*, 113309.

[29] A. C. Mayer, M. F. Toney, S. R. Scully, J. Rivnay, C. J. Brabec, M. Scharber, M. Koppe, M. Heeney, I. McCulloch, M. D. McGehee, *Adv. Funct. Mater.* **2009**, *19*, 1173.

[30] N. C. Miller, E. Cho, R. Gysel, C. Risko, V. Coropceanu, C. E. Miller, S. Sweetnam, A. Sellinger, M. Heeney, I. McCulloch, J.-L. Brédas, M. F. Toney, M. D. McGehee, *Adv. Energy Mater.* **2012**, *2*, 1208.

[31] K. Vandewal, W. D. Oosterbaan, S. Bertho, V. Vrindts, A. Gadisa, L. Lutsen, D. Vanderzande, J. V. Manca, *Appl. Phys. Lett.* **2009**, *95*, 123303.

[32] L. A. A. Pettersson, L. S. Roman, O. Inganäs, *J. Appl. Phys.* **1999**, *86*, 487.

[33] K. H. Hendriks, W. Li, M. M. Wienk, R. A. J. Janssen, *J. Am. Chem. Soc.* **2014**, *136*, 12130.

[34] Y. Yu, F. Yang, Y. Ji, Y. Wu, A. Zhang, C. Li, W. Li, *J. Mater. Chem. C* **2016**, *4*, 4134.

[35] A. Armin, M. Hambsch, I. K. Kim, P. L. Burn, P. Meredith, E. B. Namdas, *Laser Photonics Rev.* **2014**, *8*, 924.

[36] F. Guo, Z. Xiao, J. Huang, *Adv. Opt. Mater.* **2013**, *1*, 289.

[37] G. Lakhwani, A. Rao, R. H. Friend, *Annu. Rev. Phys. Chem.* **2014**, *65*, 557.

[38] C. Yang, P. Tsai, S. Horng, K. Lee, S. Tzeng, H. Meng, J. Shy, C. Shu, *Appl. Phys. Lett.* **2005**, *87*, 181108.

[39] Z. Tang, A. Elfwing, A. Melianas, J. Bergqvist, Q. Bao, O. Inganäs, *J. Mater. Chem. A* **2015**, *3*, 24289.

[40] F. C. Krebs, *Sol. Energy Mater. Sol. Cells* **2009**, *93*, 394.

[41] C.-M. Yang, P.-Y. Tsai, S.-F. Horng, K.-C. Lee, S.-R. Tzeng, H.-F. Menga, J.-T. Shy, C.-F. Shu, *Appl. Phys. Lett.* **2008**, *92*, 083504.

[42] X. Gong, M. Tong, Y. Xia, W. Cai, J. S. Moon, Y. Cao, G. Yu, C.-L. Shieh, B. Nilsson, A. J. Heeger, *Science* **2009**, *325*, 1665.

[43] M. S. Arnold, J. D. Zimmerman, C. K. Renshaw, X. Xu, R. R. Lunt, C. M. Austin, S. R. Forrest, *Nano Lett.* **2009**, *9*, 3354.

[44] J. D. Zimmerman, E. K. Yu, V. V. Diev, K. Hanson, M. E. Thompson, S. R. Forrest, *Org. Electron.* **2011**, *12*, 869.

[45] M. Young, J. Suddard-Bangsund, T. J. Patrick, N. Pajares, C. J. Traverse, M. C. Barr, S. Y. Lunt, R. R. Lunt, *Adv. Opt. Mater.* **2016**, *4*, 1028.

[46] A. London, L. Huang, B. Zhang, B. Oviedo, J. Tropp, W. Yao, Z. Wu, B. Wong, T. N. Ng, J. D. Azoulay, *Polym. Chem.* **2017**, *8*, 2922.